JOURNAL OF MATERIALS SCIENCE 26 (1991) 6011–6015

Formation mechanism of $Fe_{80}Si_8B_{12}$ metallic glass

SEONG GYOON KIM
Department of Materials Science and Engineering, Kunsan National College, Kunsan 573110, Korea

NAE EUNG LEE, HYUNG YONG RA
Department of Metallurgical Engineering, College of Engineering, Seoul National University, Seoul 151742, Korea

In order to gain an understanding of the glass-forming mechanism during the rapid quenching of a metallic alloy, the nucleation and growth process of the crystalline phase which competes with the metallic glass must be investigated. The microstructures of melt-spun $Fe_{80}Si_8B_{12}$ alloy ribbons with different thicknesses were examined using optical and electron microscopy. The phase competing with the metallic glass is α-(Fe, Si) ferrite, nucleated by the homogeneous nucleation. The growth process of α-(Fe, Si) dendrites was explained well by Lipton *et al.*'s theory of dendritic growth in an undercooled alloy melt. It was concluded that the easy glass-forming ability during rapid quenching of the $Fe_{80}Si_8B_{12}$ alloy is due to (i) the slow growth rate of α-(Fe, Si) dendrite, and (ii) the wide gap between the temperatures of the maximum nucleation rate and the maximum growth velocity.

1. Introduction

In order to understand the glass-forming ability during rapid quenching of an alloy melt, it is necessary to identify the nucleation and growth process of crystals competing with the metallic glass. Metallic glasses can be formed in the case of negligible nucleation or the slow growth velocity of crystals even if nucleation occurs. Since Uhlmann [1] and Boettinger's [2] studies to determine whether or not metallic glass is formed, several models considering the nucleation and growth process simultaneously for a given condition have been suggested [3–6]. However, these models did not consider the phase competing with the metallic glass and used the growth theory which can be applied to the massive solidification.

A detailed investigation of the phase competing with the metallic glass must, therefore, be made to gain an understanding of the glass-forming mechanism (i.e. the mechanism whereby a crystalline phase is suppressed). The phases competing with the metallic glass were examined in Fe–B, Co–B, Ni–B, (Fe, Ni)–B, (Fe, Co)–B, [7] and Cu–Ti [8] alloy systems. Among these systems, with the exception of the phase competing with the metallic glass in the Cu–Ti alloy system, which is the massive phase, that in the other alloy systems is dendritic or eutectic phase, according to composition.

The purpose of this work was to verify the glass-forming mechanism by elucidating the nucleation and growth process of the phase competing with the metallic glass in the $Fe_{80}Si_8B_{12}$ metallic alloy.

2. Experimental procedure

Rod-shape ingots of $Fe_{80}Si_8B_{12}$ alloy were prepared by induction melting. A melt spinner was used as the rapid solidification instrument. After inserting about 10 g $Fe_{80}Si_8B_{12}$ alloy in a quartz tube and melting it in the induction furnace, the crystalline and amorphous $Fe_{80}Si_8B_{12}$ alloy was produced by ejecting alloy melt on to a 15 cm diameter high-speed copper wheel. By controlling the quartz tube orifice diameter and the rotation speed of the copper wheel, ribbons 20 to 100 μm thick having different cooling rates, were obtained. After the melt-spun ribbons were polished and etched in 10% Nital solution, the overall structure was observed by optical microscopy. The microstructure of the crystals formed in the melt-spun ribbons was observed using a transmission electron microscope operating at an accelerating voltage of 200 kV. The TEM specimens were thinned from both sides in a twin-jet electropolisher using ethanol-perchloric acid (20%) solution at $-20\,^{\circ}C$.

3. Results and discussion

3.1. Solidification structure

Fig. 1 shows the cross-sectional micrograph of $Fe_{80}Si_8B_{12}$ alloy of the ribbon thickness (a) 70 μm, (b) 50 μm and (c) 20 μm. The free surface of the ribbon, the upper region in Fig. 1(a), is completely crystallized. However, in the lower region in contact with the copper wheel, crystals were not observed by optical microscopy. In the central region, the fact that

0022–2461/91 $03.00 + .12

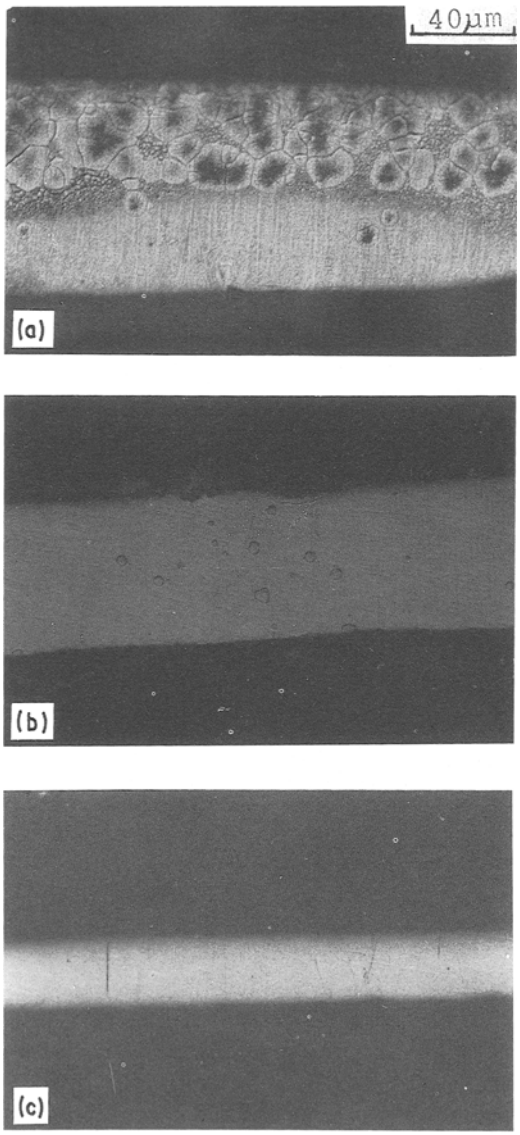

Figure 1 The microstructure of rapidly quenched $Fe_{80}Si_8B_{12}$ alloy of ribbon thickness (a) 70 μm, (b) 50 μm, (c) 20 μm.

the inside of the crystals is very etched means that the internal microstructure is coarser than that of the external microstructure. The severe change of solidification structure with position over the cross-section of the 70 μm thick specimen indicates a nonuniform cooling rate inside the sample on quenching, i.e. non-Newtonian cooling [9] occurred in this sample. Fig. 1(b) shows the cross-section of the 50 μm thick specimen. In this sample, the crystals are uniformly distributed across the whole section. From Fig. 1(c), showing the microstructure of the 20 μm thick specimen, it was found through X-ray tests and TEM observations that only the glass phase exists in this sample.

Fig. 2 shows a transmission electron micrograph of a crystal in the 50 μm thick specimen. This crystal is known to be α-(Fe, Si) ferrite from the selected-area diffraction pattern. This dendritic crystal becomes finer as crystal growth proceeds, thus as a crystal grows, the solid-liquid interface temperature decreases. This phenomenon is contrary to the case in crystalline alloys in general. Observation of the rapid solidification of crystalline aluminium alloy systems,

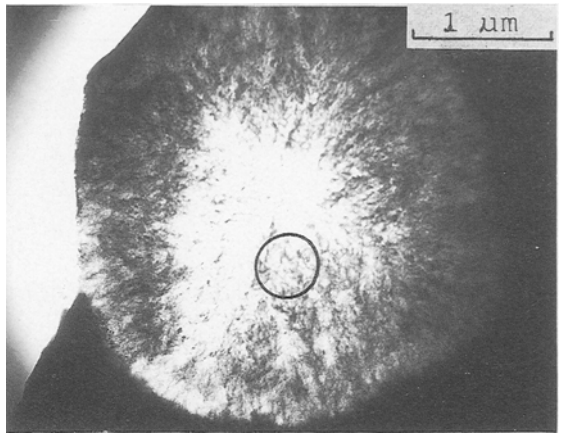

Figure 2 A typical crystal in rapidly quenched $Fe_{80}Si_8B_{12}$ alloy ribbon.

on which many studies have been made, indicates that when the nucleated crystal grows, the liquid–solid interface temperature increases by the release of latent heat of solidification, and its structure becomes coarse [9]. The difference between the microstructures of rapidly solidified $Fe_{80}Si_8B_{12}$ alloy and aluminium alloy systems can be explained by comparing their crystal growth velocities.

The size of crystals in Fig. 1 is 1 to 10 μm and these crystals would grow over a temperature range of 100 K. If we consider that the cooling rate during melt spinning is 10^5 to 10^6 K sec^{-1} [10], it takes 10^{-3} to 10^{-4} sec for these crystals to grow. Therefore, the average growth velocity of the crystal during rapid quenching can be estimated to be 0.1 to 10 cm sec^{-1}. This is very low compared with the crystal growth velocity in the melt spinning of aluminiun alloy systems [9]. In this case, the ratio of the release rate of latent heat (this value is proportional to the growth velocity) to the extraction rate of latent heat is so small that the recalescence effect of latent heat is predicted to be small. This explains why the solid–liquid interface temperature decreases on cooling the specimen and its structure becomes finer as a crystal grows.

Fig. 3(a) shows a magnified micrograph of the surrounding area of a larger crystal in Fig. 2. From its selected-area diffraction pattern, it is known that only α-(Fe, Si) microcrystals of about 50 nm in size exist. As seen in the marked area of Fig. 3(a), α-(Fe, Si) microcrystals grow with a dendrite-like morphology. Because these crystals are much smaller than those in Fig. 2, they are thought to be formed after separation from the wheel during rapid quenching. The number density of these microcrystals is 10^{21} to 10^{22} m^{-3}. According to Bergmann *et al.*'s data [4], during the manufacture of metallic glass by melt spinning, the temperature of the specimen after separation from the wheel is 700 K in the 20 μm specimen and 900 K in the 50 μm specimen and these specimens are retained for about 0.1 sec around these temperatures. Therefore, we deduced from Fig. 3(a) that the nucleation rate of α-(Fe, Si) is 10^{22} to 10^{23} m^{-3} sec^{-1}. Because of this large nucleation rate, the α-(Fe, Si) microcrystals in Fig. 3(a) are thought to be formed by homogeneous nucleation.

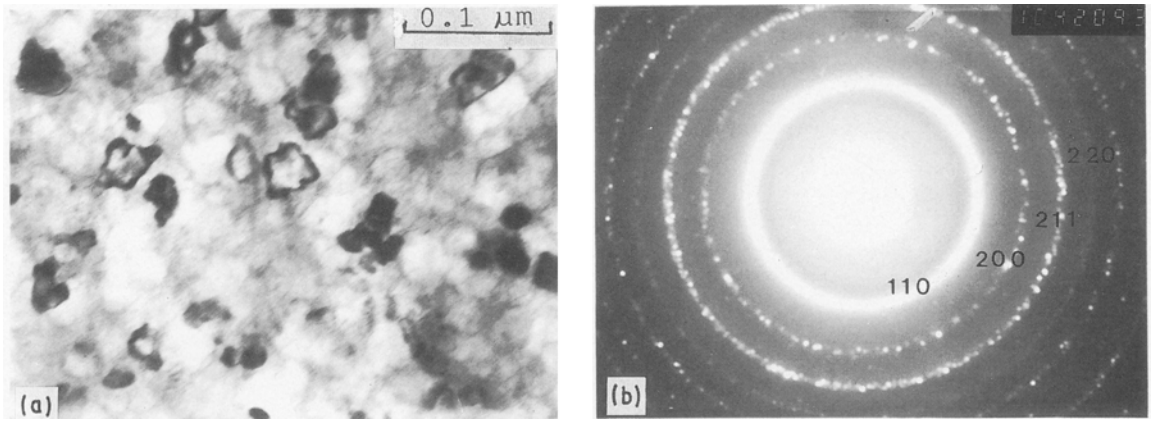

Figure 3 Fine crystals in $Fe_{80}Si_8B_{12}$ alloy ribbon (50 μm thick) and its selected area diffraction pattern.

3.2. Suppression mechanism of crystalline phase formation

As discussed in Section 3.1., the phase competing with the metallic glass during the rapid quenching of $Fe_{80}Si_8B_{12}$ alloy is α-(Fe, Si) dendrite. The nucleation rate of α-(Fe, Si) at about 900 K is very high (10^{22} to 10^{23} m^{-3} sec^{-1}), but the growth velocity is very low compared with the rapid solidification of aluminium alloy systems. From these facts, it is thought that the reason for the formation of $Fe_{80}S_8B_{12}$ metallic glass is that nucleation occurs easily, but the growth velocity of the nucleated crystal is low. However, because the nucleation rate and growth velocity change markedly during undercooling, the temperature dependence of these values must be known in order to understand the formation mechanism of metallic glass, i.e. the suppression mechanism of crystalline phase formation.

The nucleation rate, I, with undercooling can be represented as [11]

$$I = 1.654(\gamma/KT)^{1/2}N^{2/3}\nu\exp\left[-\frac{16}{3}\pi\frac{\gamma^3}{KT(\Delta G_v)^2}\right] \quad (1)$$

where γ is the solid–liquid interface energy, N the number of atoms per unit volume, ΔG_v the free energy difference between metallic glass and crystalline phase and ν the number of atomic jumps per unit time (jumping frequency). In order to obtain ΔG_v in Equation 1, the difference between specific heat of the liquid and solid phases, ΔC_p, is required. However, no experimental data for ΔC_p in the $Fe_{80}Si_8B_{12}$ alloy exist. Among the equations estimating ΔG_v, those that do not require ΔC_p are given by Hoffman [12], Turnbull [13] and Thompson and Spaepen [14]. Here Thompson and Spaepen's equation is used because it is known that this equation agrees relatively well with the experimental value [15]. Thompson and Spaepen's equation is [14]

$$\Delta G_v = \frac{2T_r\Delta T_r\Delta H_f}{(T_r+1)V_m} \quad (2)$$

where T_r is the reduced temperature (T/T_f), T_f the melting temperature, ΔH_f the latent heat of fusion at the melting temperature, V_m the molar volume, and $\Delta T_r = 1 - T_r$.

The value of $\nu = D/\lambda^2$ (where D is the diffusion coefficient and λ the jumping distance of atoms), an important variable in Equation 1, has not been reported for the $Fe_{80}Si_8B_{12}$ alloy. Viscosity measured in $Ni_{74.5}Si_{8.5}B_{17}$ alloy [16] may be similar to the viscosity of the $Fe_{80}Si_8B_{12}$ alloy. The temperature dependence of viscosity well satisfied by the following Vogel–Fuhler equation

$$\eta = A\exp\left(\frac{B}{T-T_c}\right) \quad (3)$$

where A, B are constants, and T_c is the glass transition temperature. The following relationship also exists between η and D

$$D = \frac{KT}{3\pi a\eta} \quad (4)$$

where a is the average distance between atoms. Equations 3 and 4 enable us to calculate the diffusion coefficient in $Fe_{80}Si_8B_{12}$ alloy melt from the viscosity of the $Ni_{74.5}Si_{8.5}B_{17}$ alloy melt. ΔH_f of the $Ni_{74.5}Si_{8.5}B_{17}$ alloy was used [5]. T_f is the liquidus temperature of $Fe_{80}Si_8B_{12}$ alloy [17]. Except for the solid–liquid interface energy, γ, other values for calculating the nucleation rate are presented in Table I.

The temperature dependence of the nucleation rate calculated from Equation 1 at various γ values is shown in Fig. 4. As discussed in Section 3.1, the nucleation rate of α-(Fe, Si) at about 900 K is 10^{22} to 10^{23} m^{-3} sec^{-1}. In Fig. 4 the value of γ fitted to this

TABLE I Input data for the calculation of the nucleation rate in the rapidly quenched $Fe_{80}Si_8B_{12}$ alloy.

		Reference
T_f	1425 K	[17]
ΔH_f	13.3 kJ mol^{-1}	[5]
V_m	7.1 cm^3	[a]
A	2.53×10^{-5} N S m^{-2}	[16]
B	4280 K	[16]
T_c	670 K	[16]

[a] Molar volume of pure iron.

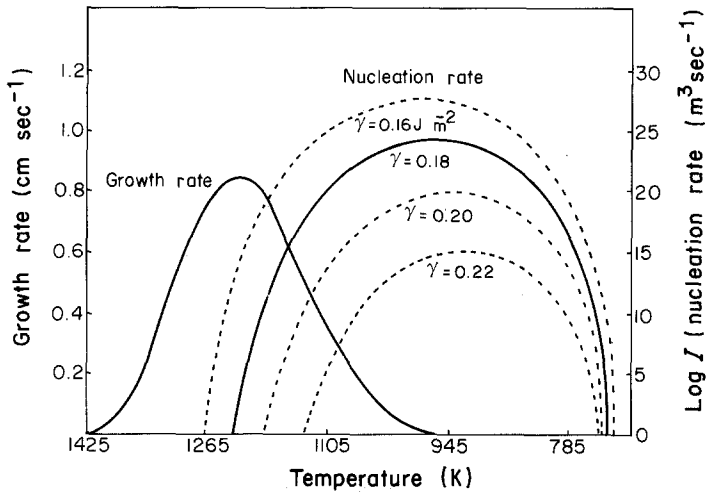

Figure 4 Nucleation and growth rate of α-(Fe, Si) with temperature calculated from Equations 1, 5 and 6.

nucleation rate is 0.18 J m^{-2}. This is similar to that of the solid–liquid interface energy in pure iron, 0.205 J m^{-2} [18].

The theory of dendritic growth in an undercooled alloy melt was suggested by Laxmanann [19] and Lipton *et al.* [20]. Laxmanann modified Burden and Hunt's dendritic growth theory [21] by combining it with the maximum growth velocity assumption [22] Lipton *et al.*,'s model [20] was made by combining Ivantsov's dendrite growth theory [23] with the marginal stability condition [24]. In this paper Lipton *et al.*'s model was used. When dendritic growth occurs in an alloy melt, the diffusion of solute atoms and latent heat occurs simultaneously.

Lipton *et al.*'s model [20], which is expressed by the dendritic growth velocity, V, and the dendrite tip radius, R, with undercooling ΔT (the difference between the liquidus temperature, T_1 and the liquid temperature far from the dendrite tip T_∞), can be represented by the following two equations [20]

$$\Delta T = mC_0\left[1 - \frac{1}{1 - I_v(P)}\right] + I_v(P_{th})\frac{\Delta H_f}{C_p} + \frac{2\gamma}{R} \quad (5)$$

$$R = 4\pi^2\left[T\Big/(\Delta H_f/C_p)P_{th} - mC_0\xi_c P\frac{1}{1 - I_v(P)}\right] \quad (6)$$

where m is the slope of the liquidus line, C_0 the bulk composition, ΔH_f the latent heat of fusion, C_p the specific heat of the liquid phase, $\Gamma = \gamma T_f/\Delta H_f$, γ the liquid–solid interface energy, $P = VR/2D$, $P_{th} = VR/2D_{th}$, D_{th} is the thermal diffusivity in the liquid phase, and

$$I_v(x) = xe^xE_1(x), \quad E_1(x) = \int_x^\infty \frac{e^{-t}}{t}dt$$

$$\xi_c = 1 - \frac{2K}{[1 + (2\pi/P)^2]^{1/2} - 1 + 2K}$$

where K is the solute distribution coefficient.

Equation 5 shows that the growth velocity of the dendrite is governed by the diffusion rate of the solute and the latent heat, and Equation 6 indicates that the dendrite is in the marginally stable state. Solving Equations 5 and 6 simultaneously enables us to obtain the growth velocity of the dendrite, V, and the tip radius of the dendrite, R, under a given undercooling, ΔT. During the rapid quenching of $Fe_{80}Si_8B_{12}$ alloy, silicon is completely soluble in α-Fe but boron is virtually insoluble in α-Fe [25]. Therefore, the solute distribution coefficient, K, becomes zero and $\xi_c = 1$. We used the slope of the liquidus line, $m = 20$ K/at %, which is obtained from the Fe–B binary diagram [26] at $X_B = 8$ at %, and D_{th} and C_p were measured from the $Ni_{74.5}Si_{8.5}B_{17}$ alloy [6]. By numerical analysis using the above data, we obtained solutions of Equations 5 and 6. In numerical analysis, $E_1(x)$ was calculated approximately from Abramowitz's integral table [25]. This approximation is sufficient for the purpose of this paper.

The growth velocity of α-(Fe, Si) dendrites with undercooling, ΔT is shown in Fig. 4. The maximum growth velocity of the dendrite is 0.85 cm sec^{-1}. This value agrees well with the mean growth velocity approximated in Section 3.2, 0.1 to 10 cm sec^{-1}. As seen in Fig. 4, the growth velocity of the dendrite is maximum at about 1225 K but the nucleation rate is maximum at about 945 K. The nucleation rate is low at the maximum growth temperature, whereas the growth velocity is low at the maximum nucleation temperature. Therefore, during the rapid quenching of $Fe_{80}Si_8B_{12}$ alloy, the formation of metallic glass is possible because of the following reasons: (1) the growth velocity of the dendrite competing with the metallic glass phase is very low; (2) the temperature of the maximum growth velocity differs from that of the maximum nucleation rate by about 300 K.

Fig. 5 shows the calculated values of $T_\infty - T_t$ (T_∞ is the liquid temperature far from the dendrite tip and T_t the temperature at the dendrite tip) and the dendrite tip radius, R, with undercooling. $T_t \simeq T_\infty$ is satisfied for the whole solidification period. Thus the low growth velocity of the dendrite does not allow released latent heat to accumulate at the liquid–solid interface. Therefore, released latent heat diffuses into the liquid phase completely. Fig. 5 shows that despite the release of latent heat, the solid–liquid interface temperature decreases as a crystal grows. This result supports the fact discussed in Section 3.1 that the structure of the dendrite becomes finer as the dendrite grows.

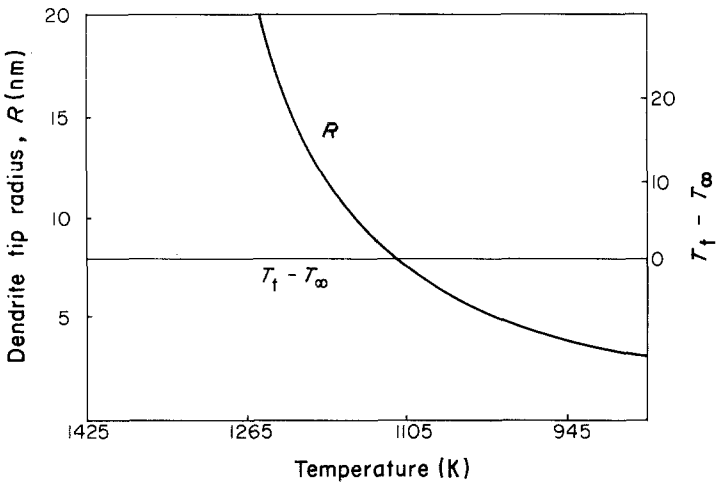

Figure 5 Dendrite tip radius and tip undercooling as a function of the bulk temperature (calculated from Equations 5 and 6).

4. Conclusions

Comparing our experimental results with the homogeneous nucleation theory and Lipton *et al.*'s dendritic growth theory [20], the following conclusions were drawn.

1. The phase competing with the glass phase is α-(Fe, Si) dendrite.

2. The microstructure of the dendrite becomes finer as the dendrite grows, because the thermal diffusion rate is much higher than the growth velocity of the dendrite.

3. The solid–liquid interface energy obtained by comparing our experimental results with the homogeneous nucleation theory, is 0.18 $J m^{-2}$.

4. The change in the microstructure and the growth velocity of α-(Fe, Si) dendrite with undercooling obtained from Lipton *et al.*'s dendritic growth theory is consistent with our experimental results.

5. The easy glass formation of $Fe_{80}Si_8B_{12}$ alloy can be explained by (i) the slow growth velocity of the dendrite competing with metallic glass, and (ii) the difference between the maximum nucleation temperature and the maximum growth temperature, which is about 300 K.

References

1. D. R. UHLMANN, *J. Non-Cryst. Solids* **7** (1972) 337.
2. W. J. BOETTINGER, in "Rapidly Solidified Amorphous and Crystalline Alloys", edited by B. H. Kear *et al.* (Elsevier, New York, 1982) p. 15.
3. P. M. ANDERSON III, J. STEINBERG and A. E. LORD Jr, *J. Non-Cryst. Solids* **34** (1979) 267.
4. H. W. BERGMANN, H. U. FRITSCH and G. HUNGER, *J. Mater. Sci.* **16** (1981) 1935.
5. D. G. MORRIS, *Acta Metall.* **31** (1983) 1479.
6. R. SELLGER and W. LÖSER, *ibid.* **34** (1986) 831.
7. J. L. WALTER, J. D. LIVINGSTON and A. M. DAVIS, *Mater. Sci. Engng* **49** (1981) 47.
8. T. B. MASSALSKI and C. G. WOYCHIK, *Acta Metall.* **33** (1985) 1873.
9. R. MEHRABIAN, *Int. Met. Rev.* **28** (1982) 185.
10. C. G. LEVI and R. MEHRABIAN, *Metall. Trans.* **13A** (1982) 221.
11. D. KASHCHIEV, *Surf. Sci.* **4** (1966) 209.
12. J. D. HOFFMAN, *J. Chem. Phys.* **29** (1958) 1192.
13. D. TURNBULL, *J. Appl. Phys.* **21** (1950) 1022.
14. C. V. THOMPSON and F. SPAEPEN, *Acta Metall.* **27** (1979) 1855.
15. K. S. DUBEY and P. RAMACHANDRARAO, *ibid.* **31** (1984) 91.
16. R. A. GRANGE and J. K. KIEFER, *Trans. Amer. Soc. Metals* **29** (1941) 526.
17. T. YAMASAKI and Y. OGINO, *J. Jpn Inst. Metals* **50** (1986) 595.
18. L. E. MURR, "Interfacial Phenomena in Metals and Alloys" (Addison-Wesley, London, 1985) p. 155.
19. V. LAXMANANN, *Acta Metall.* **33** (1985) 1023.
20. J. LIPTON, M. E. GLICKSMANN and W. KURZ, *Mater. Sci. Engng* **65** (1984) 57.
21. M. H. BURDEN and J. D. HUNT, *J. Crystal Growth* **22** (1974) 99.
22. M. E. GLICKSMANN and R. J. SCHAEFER, *ibid.* **2** (1968) 239.
23. G. HORVAY and J. W. CAHN, *Acta Metall.* **9** (1961) 695.
24. J. S. LANGER and H. MÜLLER-KRUMBHAAR, *ibid.* **26** (1978) 1981.
25. C. J. LIN and F. SPAEPEN, *Scripta Metall.* **17** (1982) 1259.
26. C. J. SMITHELL, "Metals Reference Book" (Butterworth, London, 1976) p. 469.
27. M. ABRAMOWITZ, "Handbook of Mathematical Functions" (National Bureau of Standards, Washington, D.C., 1965) p. 231.

Received 1 June
and accepted 23 October 1989